Fluid Interface Phenomena in a Low-Gravity Environment: Recent Results from Drop Tower Experimentation

Mark M. Weislogel

NASA Lewis Research Center

Cleveland, OH, 44135 USA

Shortened title: **Low-Gravity Interfacial Phenomena**

Author's full address:

Mark M. Weislogel

NASA Lewis Research Center M.S. 500/102

21000 Brookpark Rd.

Cleveland, OH, 44135 USA

ph: 1-216-433-2877

FAX: 1-216-433-8050

Email: mark.weislogel@lerc.nasa.gov

keywords: drop towers, capillary flow, contact angle, contact line, microgravity, low gravity

Fluid Interface Phenomena in a Low-Gravity Environment:
Recent Results from Drop Tower Experimentation

Mark M. Weislogel

NASA Lewis Research Center

Cleveland, OH, 44135 USA

keywords: drop towers, capillary flow, contact angle, contact line, microgravity, low gravity

ABSTRACT

Drop towers used as experimental facilities have played a major role in the development of fundamental theory, engineering analysis, and the proofing of system designs applicable to fluid interface phenomena in a low-gravity environment. In this paper, the parameters essential to the effective use of drop tower experiments relevant to fluid interfaces with constant fluid properties are reviewed. The often dramatic influence of the contact angle and the uncertainty of the moving contact line boundary condition are emphasized. A number of sample problems buttressed by recent results from drop tower tests are discussed; these clearly demonstrate the role of inertia and the controlling influence of surface wettability and container geometry for the large length scale capillary flows that arise in fluid systems in space.

1 INTRODUCTION

Fluid interface phenomena in a low-gravity (low-g) environment has remained an important area of study since the inception of spaceflight. Shortly after the success of Sputnik, a large community of engineers and scientists began to consider the practical and intriguing questions relevant to applications in low-g. To develop techniques for studying such phenomena without actually going to space, NASA constructed its first drop tower for space-related research at the Lewis Research Center in 1956. As an indication of how eager investigators in the United States were to learn the effects of low-g, three other drop towers were built later that year by industry and academia. It is no surprise that chief among the first topics of concern was fluid interface behavior [1]–[5]. After all, how would a liquid propellant behave in the fuel tank of an orbiting spacecraft? And how could systems be designed such that the desired performance was guaranteed?

Such questions were answered rapidly during what might be called the heyday of drop tower research in the U.S. (1956-1970); fluid interface phenomena in a low-g environment was found to be

little different than capillary phenomena in a terrestrial environment, the primary difference being the length scale over which capillary forces control the fluid behavior. The conclusion drawn from early observations is now as obvious as it is challenging: low-g fluid systems designs *must* accurately account for capillarity over very large length scales.

Examples of such systems can be found in most, if not all, in-space fluids management processes [6], from the positioning, control, and transport of liquids, such as fuels in storage tanks, to thermal systems such as heat pipes and capillary pumped loops, or the storage and handling of biological fluids and wastes. In addition, requirements of space experiments featuring fluid interfaces (e.g., see Ref. [7]-[9] and experiments cited therein) have provided new applications for our knowledge of capillary phenomena. Notable examples of problem areas are the behavior of drops and bubbles, the formation of liquid bridges, the use of pinning lips to stabilize interfaces, the filling and draining of irregular containers with partially wetting liquids, and the stabilization of irregular interface configurations against adverse disturbances. Recent efforts toward investigating problems of a more fundamental nature are also being pursued on an international level [10]. Despite a limited experiment duration, drop towers continue to play a significant role in the testing of such fluid systems designs and in the development of engineering tools to predict fluid behavior in a low-g environment.

In this paper, the controlling parameters describing the general behavior of fluid interfaces in a low-g environment are reviewed. A selection of design parameters helpful in scaling experiments to take advantage of the brief time afforded by a typical drop tower is then given. Next, several example problems are given to illustrate surface reorientation and settling during transition from "high-g" to low-g, the control of capillary surfaces by varying surface wettability, and the control of fluids by using specific container geometry. Each example is supported by recent experimental results obtained in a drop tower. Lastly, a word of caution concerning the use of drop towers and the interpretation of drop tower data is offered.

2 REVIEW OF PARAMETERS

A brief introduction to the controlling parameters of fluid interfaces with constant thermophysical properties is necessary in order to provide the basis for static and dynamic similitude between scaled drop tower experiments and the full-sized systems they are intended to mimic (see also Ref. [11]). The parameters to be discussed are equally useful as engineering tools for predicting fluid characteristics. Static interface shape problems, forced flows, and spontaneous capillary flows are considered. In all cases a rigid container partially filled with liquid and a nonparticipating gas phase is assumed.

2.1 Scaling Parameters

A measure of the strength of body forces (e.g., gravity) compared to capillary forces (i.e., surface tension) is given by the Bond number

$$Bo = \frac{\rho g R^2}{\sigma} \tag{1}$$

where ρ is the density of the liquid, g is the acceleration field strength (gravity), R is a characteristic dimension of the interface or container, and σ is the surface tension. When $Bo \ll 1$, surface tension forces dominate the fluid behavior. For fixed fluid properties, $Bo \ll 1$ can be assured if either R or g is small. Since $g = g_o$ is fixed on Earth, $R \lesssim 1$ mm for typical fluids. However, aboard orbiting spacecraft, where $g \sim 10^{-6} g_o$ is common, the system length scale can increase to $R \lesssim 1$m (1000-fold its normal-g analog!) while maintaining $Bo \ll 1$.

When $Bo \sim 1$, body forces and surface tension forces are in balance. Larger values of Bo, perhaps due to an unfavorable magnitude and orientation of the acceleration field, can lead to destabilization of the interface and breakup and/or flow to a new location within the container [12]–[16].

A ratio of inertial forces (i.e., convection) to surface tension forces is given by the Weber number

$$We = \frac{\rho R V^2}{\sigma} \tag{2}$$

where V is the characteristic velocity of the fluid. When $Bo \ll 1$, $We \sim 1$ is the balance point. With larger values the surface is likely to break-up because of convective flows [5]. Similarly, a balance between viscous and surface tension forces is given by the capillary number

$$Ca = \frac{\mu V}{\sigma} \tag{3}$$

where μ is the dynamic viscosity of the liquid. When $Bo \ll 1$, Ca is a measure of the degree of distortion and stability of an interface that are due to viscosity.

For spontaneous capillary flows, the velocity scale depends primarily on the balance between surface tension and viscosity, or $Ca \sim 1$; thus $V \sim \sigma/\mu$. Substituting this scale into Eq. (2) yields

$$Su = \frac{\rho \sigma R}{\mu^2} \tag{4}$$

where Su is the Suratman number which serves as a measure of inertia in a capillary system ($Su = Oh^{-2}$, where Oh is the Ohnesorge number). Therefore, for fixed fluid properties, because the low-g limit permits dramatic increases in system size R, while maintaining $Bo \ll 1$, the inertia in capillary flows similarly increases since $Su \propto R$. Significant inertia is perhaps the most distinguishing characteristic of low-g capillary flows with constant properties.

2.2 Similitude

Eqs. (1) to (4) form a primary set for scaling full-sized system designs for testing in drop towers. Matching Bo, or at least ensuring $Bo \ll 1$, will duplicate interface statics. When $Bo \ll 1$, dynamics can be simulated by matching either We, in the case of forced inviscid flow, or Su in the case of spontaneous capillary flow. In all cases, the wetting conditions (contact angle) must be matched, the importance of this will be clarified shortly. To mimic dynamic curvature effects produced in the vicinity of the moving contact line, Ca should also be considered.

To exploit the brief experiment time afforded by typical drop towers, test fluids should be selected judiciously by matching the particular parameters of interest, while giving ample consideration to the time scales involved in the transition from 1-g to low-g. Several important time scales [17] are

1. Viscous time scale, $t_\mu \sim \rho R^2 / \mu$: Time necessary for bulk fluid to assume viscous flow.

2. Inertial time scale, $t_R \sim (\rho R^3 / \sigma)^{1/2}$: Time for a capillary surface to form after rapid reduction in gravity level. Also the approximate natural period of oscillation for a perturbed interface.

3. Capillary flow time scale, $t_\sigma \sim \mu R / \sigma$: Characteristic set-up time for a capillary driven flow.

Clearly all time scales increase with container size. Thus, effective drop tower experiments relating to capillary phenomena are usually scaled-down appreciably so that R is on the order of centimeters or less. Note also that t_μ decreases with increasing viscosity μ while t_σ increases with increasing viscosity. This reciprocal relationship with μ often requires some compromise in the selection of fluids for effective drop tower experimentation. The above time scales will be discussed further in section 3.

2.3 Significance of the Contact Line

In predicting static interface behavior, it is most insightful to recognize that once the condition $Bo \ll 1$ is achieved, surface tension plays no role! In fact, even in many capillary flow scenarios in a low-g environment, surface tension enters the problem only by affecting the rate at which the flow proceeds. Actually, the static fluid interface depends on the system geometry and the surface wettability, the latter being characterized by the contact angle θ.

In the case of a liquid partially filling a rigid container, the contact angle serves as the measure of the wettability of the solid by the liquid. The condition $\theta = 0$ is considered a perfectly wetting condition, whereas $\theta = 180°$ is considered perfectly nonwetting. Figure 1 depicts a circular cylindrical container with several interfaces (menisci) satisfying $Bo \ll 1$ for a variety of contact angles. Each surface is a portion of a sphere. Because both the sign and magnitude of the pressure drop across

the meniscus are dependent on its curvature, the contact angle controls not only the interface shape [18], but also the favored direction in which flow can be expected. In this way the contact angle has a direct impact on the dynamics and stability of the interface. Though this is not necessarily a dramatic observation for terrestrial applications, in low-g, where liquid fuel inventories can account for over 50% of a satellite's mass [19], the contact angle condition can play a dramatic role indeed! In such a system, an unknown or uncontrolled oscillation of the liquid could prove disastrous [20].

The contact angle is often considered a macroscopic thermodynamic property of the system [21]. However, for larger values, for systems with nonidealized surfaces and/or fluids, the contact angle is hysteretic, and the correct angle depends rather on the history of the contact line than on a single-valued equilibrium measurement.

The contact line is the three-phase line (region) where the contact angle boundary condition is applicable (see Fig. 1). For static interfaces, the microscopic region is complex, system dependent, and often time dependent ([22], p. 328). Even more difficulties arise when the contact line moves [22][23]: (1) the physical mechanisms are uncertain; (2) a stress singularity results when the classical no-slip condition is applied along the wall; and (3) numerical analyses are hampered when interface behavior is predicted without the correct boundary condition at the contact line. Because of the combined uncertainty *and* importance of the correct contact line condition, further research along this vein is necessary in order to advance our understanding of the fundamental mechanisms involved. Without such advances, truly predictive models of fluid interface behavior on Earth as well as in space are limited to certain restrictive cases or empiricism. This fact should be evident from the tests selected for discussion herein. The literature offers a number of interesting works related to the more physical aspects of the moving contact line [24]–[27]. For modeling purposes applicable to low-g flows, see References [3][22] and [28]–[32] and the references contained therein. It is astonishing that applications in capillary phenomena in a low-g environment continue to be overlooked in the literature [33].

3 Example Problems

Three example problems highlighting low-g interfacial phenomena are presented here. The intent is to quantitatively describe flows which illustrate several key characteristics of spontaneous capillary flows that may be systematically studied by using drop towers. These characteristics include the transient role of inertia, the controlling influence of the contact angle and moving contact line, and the impact of container geometry. Each example stems from applications arising from drop tower experiment design, spaceflight experiment design, or spaceflight systems design. Each example is

also supported with data acquired using a 2.2-s drop tower at NASA's Lewis Research Center [34].

3.1   Interface Settling after a Step Reduction in Gravity

The rapid reduction in gravity level characteristic of most drop towers can result in a global reorientation or redistribution of fluids within partially filled containers. For fixed container geometry, the degree of reorientation is dependent only on the contact angle of the particular fluid-solid pair and the change in system Bond number. (An instantaneous reduction in g-level will be assumed in the discussion to follow.) If the reduction in gravity level is such that $Bo \gg 1$ prior to the drop and $Bo \ll 1$ after release, significant reorientation of the fluid can be expected during the transition between 1-g and low-g. For example, such a transition for a circular cylindrical container partially filled with a liquid would result in a flow from a predominantly flat interface configuration towards one of constant curvature meeting the container wall at the contact angle. These configurations are depicted in Figure 2 for a perfectly wetting fluid ($\theta = 0$). Depending on the damping of the system, decaying oscillations of the surface about the low-g equilibrium shape are often observed. Drop tower test data presented in Figure 3 display the surface settling history for the meniscus centerline location $Z(t)$ for a variety of viscosities (Fig. 3(a)) and contact angles (Figure 3(b)). Figure 3 shows that the frequency of oscillation increases with increasing viscosity and contact angle. The rate of decay of the oscillations is seen to increase with increasing viscosity for low contact angles ($\lesssim 40°$), but decrease with increasing viscosity for larger contact angles. For such tests the normal- and low-g equilibrium surface configurations are known [12]. However, the transients associated with the reorientation are complicated and have received little attention by way of analysis. This is understandable in that the fluid interface experiences a number of inertial regimes enroute to a transient viscous flow. For example, when $Bo \gg 1$ prior to the drop the only interfacial length scale is the capillary length $L_c = (\sigma/\rho g)^{1/2}$, which is independent of any container length scale R and serves as a measure of the region near the wall where surface tension forces are appreciable (see Fig. 2). It can be shown that the initial inertial response of the interface after a step reduction in gravity occurs within

$$t_{L_c} \sim \left(\frac{\rho L_c^3}{\sigma}\right)^{1/2} = \left(\frac{\sigma}{\rho g^3}\right)^{1/4} \tag{5}$$

Part of this initial response is the production of capillary waves of wave length L_c, which emanate from the contact line region and propagate with velocity $U_{L_c} \sim (\sigma g/\rho)^{1/4}$ across the surface. Thus, the container length scale becomes relevant after a characteristic time

$$t_{RL_c} \sim \frac{R}{U_{L_c}} \sim R\left(\frac{\rho}{\sigma g}\right)^{1/4} \tag{6}$$

7

The inertial response of the entire system then dominates and is characterized by

$$t_R \sim \left(\frac{\rho R^3}{\sigma}\right)^{1/2} \tag{7}$$

If $Bo \lesssim O(1)$ prior to release, $L_c \simeq R$ and the various inertial time regimes described by Eqs. (5) to (7) reduce to the single time scale given by Eq. (7), since in this limit $t_{L_c} \simeq t_{RL_c} \simeq t_R$.

Such inertial transients have been studied previously regarding the response of an interface in a circular cylinder to a step reduction in gravity level [35]–[39]. Unfortunately, for both theoretical and numerical analyses of the problem, during this establishment period the flow is further complicated by a developing viscous boundary layer, by the transition of surface oscillations from nonlinear to linear regimes, and by the fact that the moving contact line region becomes a key, though little understood, mechanism of dissipation for the oscillations [29][40].

Nonetheless, the frequency of oscillation and the damping rate or settling time for the free surface during this process are important characteristics, the knowledge of which aid directly the design of low-g fluids systems.[1] Since the flow is too involved for current theoretical analysis, and numerical solutions are without a correct boundary condition to apply at the contact line, empiricism remains a valued recourse to obtain quantitative information. A correlation [38] has been developed for the settling time of fluid interfaces in cylinders after a step reduction in gravity. A large parametric range of tests were performed and, based on an accompanying scale analysis, the complete data set was correlated. Subsequently, a numerical code [39] was "tuned" to reproduce a portion of these results.

If the settling time t_s is defined as the point at which regular oscillations are no longer detectable or, in the case of high viscosity fluids, the point at which the axial meniscus location stabilizes, the following relationship has been demonstrated [38] to be effective for estimating t_s:

$$\frac{\mu t_s}{\rho R^2}(1 + \Theta^2) \doteq 10^B \zeta^A + 0.01\Theta^2 \tag{8}$$

where

$$\zeta = \mu \left(\rho R \sigma \Theta^2 \cos\theta\right)^{-1/2} \tag{9}$$

$$\Theta = \frac{1 - \sin\theta}{\cos\theta}$$

$$A = -1.2\Theta^2 + 2.2\Theta + 0.28$$

$$B = 3.9A - 3.32$$

Figure 4 displays $\mu t_s(1 + \Theta^2)/\rho R^2$ versus $10^B \zeta^A + 0.01\Theta^2$ for the tests performed. Data from other sources are included on the plot. Eq. (8) for surface settling in circular cylinders upon step reduction

---

[1]The natural frequency and damping rate for the fundamental lateral slosh mode in a circular cylinder have been determined empirically [41].

in gravity permits determination of t_s to within a factor of 2 for the entire range of parameters tested: $0.0005 \leq \mu \leq 0.5$ kg/m·s; $9.52 \leq R \leq 30$ mm; $760 \leq \rho \leq 1238$ kg/m³; $0.0159 \leq \sigma \leq 0.0695$ N/m; and $0° \leq \theta \leq 70°$. For more than 85% of the data, the accuracy of Eq. (8) for t_s is better than $\pm 50\%$. For the specific case of $\theta = 0°$, Eq. (8) simplifies to

$$t_s = \frac{\rho R^2}{2\mu}\left(50\zeta^{1.28} + 0.01\right) \tag{10}$$

and is accurate to $\pm 20\%$. Sources of scatter in the data include container cleanliness, contact angle hysteresis, slight variations in initial interface configuration, and nonaxial slosh-type oscillations due to misalignment of the cylinder with the acceleration vector. Note that for $\theta = 0$, $\zeta = Su^{-1/2}$ (Su is defined by Eq. (4)). Thus, as $\zeta \to 0$ ($Su \to \infty$), $t_s \sim \rho R^2/\mu$, which is the parametric equivalent of t_μ in section 2.2.

The result of Eq. (8) is directly useful in scaling experiments for drop tower tests. It also provides guidance for rapidly estimating settling times given a general reduction in body force; the impact to spacecraft propellant tanks is analogous when engine thrust is terminated [43].

3.2   Control of Interfaces Using Surface Coatings

Because the contact angle and the conditions at the contact line play such a significant role in low-g flows it is only natural that systems designs exploit such conditions rather than merely account for them. For example, on Earth, a gradient in surface wettability (contact angle) can be used to move a small liquid drop a short distance across a substrate—even against the force of gravity [44]. In comparison, variations in surface wettability effect the movement of huge amounts of fluid in a low-g environment. Figure 5(a) depicts a spherical tank partially filled with a liquid at normal-g. The left side of the tank is treated such that the contact angle between the liquid and the tank wall is large, whereas on the right side $\theta = 0$. When the tank is dropped in a drop tower, the fluid configuration of Figure 5(a) reorients to that shown in Figure 5(b). Thus the location, configuration, and flow of a liquid in low-g can be controlled simply by varying the surface wettability.

In most cases, the static interface(s) should be determinable [45]-[47]. However, determining the rate with which the fluid moves because of changes in the system contact angle is a difficult problem requiring the solution of a 3-dimensional transient interface dominated, in fact driven, by the moving contact line. Computational methods are applicable to such problems, but, as mentioned in section 2.3, the boundary condition applied at the contact line would need to be ad hoc and the run time extensive.

The important parameters for such flows may be easily discerned from a recent study of spontaneous capillary flows in partially coated tubes [48]. In Figure 6 is sketched a circular cylindrical

capillary tube partially filled with a liquid slug. The ends of the tube are open to the atmosphere, and the left side of the tube is treated such that the condition there is less wetting than on the right side ($\theta_1 < \theta_2$). Since the pressure jump across a given interface is proportional to the curvature of that interface, a pressure gradient in the direction of the more favorably wetted side of the tube is established. If the pressure gradient overcomes hysteresis, it produces a flow resisted by the fluid's viscosity. After a brief transient, the macroscopic flow is steady and persists as long as the liquid slug bridges the wetting discontinuity.

Some experimental results are provided in Figure 7, which presents the axial location of the advancing meniscus with respect to time for a variety of liquid slug lengths l, all else held equal. These data were acquired by using small capillary tubes tested horizontally at normal-g in the manner illustrated in Figure 6. As can be seen in Figure 7, the base flow is indeed steady.

For such a simplified geometry, an analysis assuming $g = 0$, $We \ll 1$, $Ca \ll 1$, $\rho R^2/\mu t \ll 1$, and $r/l \ll 1$ yields

$$\langle V \rangle = \frac{\sigma}{4\mu M} \frac{r}{l} \Delta \cos \theta \qquad (11)$$

for the average velocity of the liquid. Here, $\Delta \cos \theta \equiv \cos \theta_1 - \cos \theta_2$, r is the tube radius, l is the length of the liquid slug, and

$$M = 1 + \frac{\mu_g}{\mu} \left(\frac{L - l}{l} \right)$$

where μ_g is the viscosity of the displaced gas and L is the tube length. Eq. (11) reveals that the speed of the liquid column is proportional to σ/μ, that the geometric dependence of the flow is characterized by $r/4Ml$, and that, most importantly, the flow is directly proportional to the difference in surface wettability $\Delta \cos \theta$. The contact angles θ_1 and θ_2 appearing in $\Delta \cos \theta$ are dynamic values and, though they are related to the static values, previous work [48] should be consulted for more descriptive coverage of the problem. Lastly, it should be noted that $\langle V \rangle \propto r$. Since r can increase 1000-fold in a low-g environment, flow rates ($\sim r^3/l$) for similar configurations can be expected to increase many orders of magnitude in the large low-g systems satisfying $Bo \ll 1$.

By defining $a \equiv r/4Ml$, Eq. (11) may be rearranged to give

$$\frac{\langle V \rangle}{\Delta \cos \theta} = \frac{a\sigma}{\mu} \qquad (12)$$

where the left and right side terms represent dependent and independent variables, respectively. Experiments performed by using small diameter ($\lesssim 2$ mm) straight capillary tubes tested horizontally at normal-g, and large diameter ($\lesssim 10$ mm) U-tubes tested in a drop tower show favorable agreement by way of Eq. (12) over a large parametric range: $0.258 \leq r \leq 4.94$ mm; $6 \leq l \leq 134$ mm; $95 \leq L \leq 481$ mm; $0.0005 \leq \mu \leq 0.1$ kg/m·s; $760 \leq \rho \leq 964$ kg/m^3; and $0.016 \leq \sigma \leq 0.021$

N/m. The static contact angle was $\theta_1 = 0$ for all tests performed, and the range of static values for θ_2 was $31° \leq \theta_2 \leq 60°$. These data are presented on log scales in Figure 8.

Scatter of the data in Figure 8 is attributable to nonuniformities in the surface conditions between tests which are denoted by initially dry, prewet with a thick film, and prewet and allowed to drain dry. Though the scatter is appreciable over the entire range of test parameters, it decreases significantly with increasing control of the surface conditions (see prewet and drain dried data on Fig. 8). Also, the general agreement with Eq. (12) appears universal for the range of $a\sigma/\mu$ tested.

The simple test configuration is unique in that it produces a spontaneous capillary flow which is *steady*. Most spontaneous capillary flows are transient ([1] and [22], p. 348). Nonetheless, in such cases one merely finds dependencies of the flow similar to those given by Eq. (11), only, in general,

$$V \sim F(\theta, \text{geom})(\sigma/\mu)^{c_1} R^{c_2} t^{-c_3} \tag{13}$$

where t is time, c_1, c_2, and c_3 are positive exponents, and $F(\theta, \text{geom})$ is a dimensionless function of the contact angle(s) (analogous to $\Delta \cos\theta$ discussed above) and the container geometry (to be further addressed below). For this unique configuration $F(\theta, \text{geom}) = a\Delta\cos\theta$, $c_1 = 1$, and $c_2 = c_3 = 0$.

3.3   Control of Interfaces by Using Container Geometry

As illustrated in Figures 1 and 2, fluid interfaces assume spherical caps in circular cylindrical containers when $Bo \ll 1$. This is true for all values of the contact angle. However, an entirely different situation can arise for a cylinder of square cross section. As is illustrated in Figure 9, rather than the fluid simply covering the base of the container as in the case of the circular section, the corners of the container act as a conduit for capillary pumping, redistributing the fluid within the container when $Bo \ll 1$ (Fig. 9(b)). This effect is a direct consequence of the container geometry—in this case, the interior corner angle and the contact angle. For example, for $0 \leq \theta \leq 45°$ the general low-g configuration of Figure 9b is correct. However, for $45° < \theta < 135°$ a configuration much like the circular cylinder results (Fig. 9(c)), and for $135° \leq \theta \leq 180°$ (Fig. 9(d)) the general configuration of Figure 9(b) is re-established, only the gas and liquid phases are reversed (see Ref. [46] and the references contained therein, see also Ref. [17][49]).

Knowing that the presence of interior corners leads to such behavior when $Bo \ll 1$ is immediately useful to low-g fluid systems design. Whether used as a method of transport or for the passive positioning of liquids in tanks or conduits, the strong influence of container geometry on capillary behavior should be exploited whenever possible. Again, static interface configurations are, to a large extent, determinable [45][46][50]. Unfortunately, the dynamics remain difficult to model and are controlled by the physics specific to the moving contact line, as discussed in section 2.3.

A simplified analysis, however, is possible for the case of a spontaneous capillary flow due to the interior corners in containers. An example test problem from which drop tower data are readily available is shown in Figure 10 for a fluid with $\theta = 0$. A container of equilateral triangular cross section is shown first in a normal-g environment prior to release in a drop tower. Gravity is suddenly eliminated and the flow proceeds up the corners to a very large height if allowed. Figure 10(b) provides a digitized overlay of the interface profiles shown in Figure 10(a).

The general requirement for such corner flows is given by the Concus-Finn condition, $\theta \leq 90° - \alpha$, where α is the half-angle of the interior corner [51]. Thus, if θ is small enough, significant interior corner flows can be achieved provided $Bo \ll 1$. By assuming a slender fluid column along the corner, it is possible to formulate the problem in terms of the height of the meniscus h measured perpendicular to the corner axis along the bisector of the corner angle (consult Ref. [52] for greater detail). Thus, $h = h(z, t)$, where z is the corner axis coordinate, and the governing equation for flow in an isolated corner is represented nondimensionally by

$$\frac{\partial h}{\partial t} = 2\left(\frac{\partial h}{\partial z}\right)^2 + h\frac{\partial^2 h}{\partial z^2} \tag{14}$$

where $h = h'/H$, $t = F_i Wt'/2L$, and $z = z'/L$, where primes denote dimensional variables. Here, H is a characteristic dimension of the interface in the corner and is also dependent on α and θ [49][52][53], L is a characteristic length of the liquid column, F_i is a weak numerically determined function of α and θ such that $1/8 \lesssim F_i \leq 1/6$, and $W = H\sigma \sin^2 \alpha/L\mu f$ is the characteristic velocity with

$$f = \left(\frac{\cos \theta}{\sin \alpha} - 1\right)^{-1} \tag{15}$$

representing the geometric driving force for the flow.

A number of insightful solutions deriving from Eq. (14) have been determined [52][54]–[58]. However, as seen in Figure 10(b), for the case of spontaneous capillary rise in a drop tower test, a condition of constant height (H, see Fig. 10(b)) is rapidly achieved at a location that is defined as the origin for the analysis. Thus, the conditions for modeling the "capillary rise" problem require that at some known origin $z \equiv 0$, $h(0, t) = 1$ [49][52][58]. Also, at the advancing tip it is assumed that $h(\mathcal{L}, t) = 0$, where $\mathcal{L} = \mathcal{L}(t)$ is the length of the liquid column from $z = 0$ to the tip. With the additional constraint of a constant fluid volume, the numerical solution to Eq. (14) yields

$$h \doteq 1 - 0.571\eta^+ - 0.429\eta^{+2} \tag{16}$$

where

$$\eta^+ = 0.415\frac{z}{t^{1/2}} \tag{17}$$

and is restricted to $-0.058 \lesssim \eta^+ \leq 1$. At the advancing tip $\eta^+ = 1$. At the receding bulk meniscus $\eta^+ \doteq -0.058$. *Redimensionalizing* these results yields (dropping primes)

$$h \doteq H \left(1 - 0.571\eta^+ - 0.429\eta^{+2}\right) \tag{18}$$

where

$$\eta^+ = 0.587 \left(\frac{\mu f}{\sigma H F_i \sin^2 \alpha}\right)^{1/2} \frac{z}{t^{1/2}} \tag{19}$$

and, for an n-sided regular polygon, using the technique of de Lazzer and Langbein [53] (see Ref. [52])

$$H = \frac{D}{2f} \frac{\sin(\alpha + \delta)}{F_{A_n}} \left[1 - \left(1 - \frac{F_{A_n} \cot \pi/n}{\sin^2(\alpha + \delta)}\right)^{1/2}\right] \tag{20}$$

where $\delta = \pi/n - \theta$, $\alpha = \pi(n - 2)/2n$, D is the face width of the polygon, and

$$F_{A_n} = \frac{\sin^2 \delta}{\tan \alpha} + \sin \delta \cos \delta - \delta$$

The entire surface $S(y, z, t)$ may then be determined by substituting Eq. (18) into

$$S = h(1 + f) + \left((hf)^2 - y^2\right)^{1/2} \tag{21}$$

where $|y| \leq hf \cos(\alpha + \theta)$. Eqs. (18) to (21) for a system identical to that for the drop tower experiment results shown in Figure 10 gives the solution for S for a step reduction in gravity level as shown in Figure 11. Quantitative comparisons show surprisingly good agreement even for small times ($t_\sigma \sim \mu D^2/\sigma H$) over a large portion of the surface. Excellent agreement is achieved over the entire surface as time increases [58]. As expected, scatter in the results is again observed especially for $\theta \neq 0$, due to surface irregularities and contamination common to most moving contact line problems.

Perhaps most educational about such flows is that though the viscous time scale for the fluid in the bulk can be large ($t_\mu \sim \rho D^2/\mu$) the flow in the bulk is controlled by the slender column flow in the corners. Although this flow may progress with high speed for a spontaneous capillary flow (~ 10 cm/s), it is nearly parallel, thus rendering inertia negligible in the corner. Therefore, though the bulk flow is not correctly modeled by the assumptions of the analysis, the removal rate of fluid from the bulk is, and the flow throughout the container is well approximated by Eqs. (18) to (21). The time to achieve a "slender column" can be demonstrated to be governed by $t_\sigma \sim \mu D^2/\sigma H$, a modification of t_σ introduced in section 2.2. The brief start-up flow prior to the establishment of the slender column may also be analyzed [52] as it passes through several inertial regimes analogous to those present during transient capillary rise between parallel plates [59].

The analysis succeeds by skirting the difficulties associated with the moving contact line because the predominant flow direction is parallel to it. This feature of the flow staves off dynamic contact

angle effects to higher order. From the analytic solution, the dimensional velocity of the advancing tip is

$$V_{tip} = \frac{\partial \mathcal{L}}{\partial t} = 0.851 \left(\frac{F_i \sin^2 \alpha}{f} \right)^{1/2} \left(\frac{\sigma}{\mu} \right)^{1/2} H^{1/2} t^{-1/2} \tag{22}$$

which is organized to recover the form of Eq. (13).

4   Further Considerations for Drop Tower Research

As demonstrated in section 3, drop towers can be used effectively as tools for the systematic study of certain fluid interfacial phenomena in a low-g environment. The effectiveness of such research is based on the particular experiment time scales, outlined in part in section 2. The best quantitative results are obtained when the systems studied are sized appropriately to make optimal use of the brief low-g time afforded by the drop tower; thus equilibrium interface configurations are established, flows are steady, or fully developed, and so on. Such restrictions prevent the exploitation of the drop tower as a low-g facility for many experimental investigations.

For fluid interface experiments, the particular design of the drop tower employed may play an important role. For example, the disturbance caused by the release mechanism, the rate of release, the "ringing" of the experiment platform after release, or a non-negligible acceleration field during free-fall (i.e., drag) can all contribute to undesirable oscillations of the fluid surface. Many such disturbances are high frequency by nature and produce correspondingly high frequency capillary waves that may or may not decay within an acceptable time limit. (Bulk flows rapidly overwhelm such high frequency waves.)

Since low-g (static) interface configuration experiments are highly sensitive to the initial condition at the contact line, particularly when $\theta > 0$ the handling of the experiment prior to the drop test is also important [60]. In such cases, a statistically significant data set is necessary to ensure reproducibility within definitive limits, and the provisions of alignment, balance, and symmetry are requirements of the drop tower.

Lastly, without repeat measurements for a variety of initial interface configurations, conclusions drawn from drop tower results can be misleading. This is due to the multiple metastable interface configurations that are often possible in any given container [61][62]. This point is supported by recent results from experiments performed in collaboration with P. Concus and R. Finn in which the interface configuration of a partially filled "proboscis" container was tested both in a drop tower and in the longer duration low-g environment of the Space Shuttle [63]. Two low-g static interface configurations from the flight experiment are depicted in Figure 12. Identical results (as shown in Fig. 12(a)) are obtained whether tested in a drop tower or in space [64]. However, after sufficient time

14

(minutes) and disturbances to the container, the interface adjusts itself according to the minimum energy state determined by the particular container geometry and system contact angle. Provided ample time (days), ambient mechanical disturbances, and thermal fluctuations, the fluid in Figure 12 would continue to wrap around the lid of the container in a counter clockwise direction before halting at the top of the left side. The drop tower test duplicates only the flight result of Figure 12(a), which is a static, though metastable, interface configuration. Longer duration low-g exposure is necessary to observe the more subtle characteristics of such fluid interface problems.

ACKNOWLEDGEMENT

References

[1] R. Siegel, Transient capillary rise in reduced and zero-gravity fields, *J. Appl. Mech.*, June, 165 (1961).

[2] E.T. Benedikt, General behavior of a liquid in a zero or near zero gravity environment, Rep. ASG-TM-60-9Z6, Norair Div., Northrop Corp., May 1960.

[3] W.C. Reynolds, H.M. Satterlee, Liquid propellant behavior at low and zero g, in NASA SP-106, ed. H.N. Abramson, 1966, chpt. 11.

[4] T. Li, Hydrostatics in various gravitational fields, *J. Chem. Phys.*, 36, No. 9, May 1, 2369 (1962).

[5] H.M. Satterlee, M.P. Hollister, Low-g liquid propellant behavior, engineers handbook, LMSC-A874831, NAS 9-5174, May 1967.

[6] J.A. Salzman, Fluid management in space-based systems, Space Engineering-Construction-Operations in Space V, Proceedings of the Fifth International Conference on Space, Vol. 1, 521 (1996).

[7] P.R. Sahm, R. Jansen, M.H. Keller (eds.), Scientific Results of the German Spacelab Mission D1, Proceedings of the Norderney Symposium, Norderney, Germany, Aug. 27-29, 1986.

[8] Joint Launch + One Year Science Review of USML-1 and USMP-2 with Microgravity Measurement Group, NASA Conference Publication 3272, Vol. I and II, May, 1994; Proceedings of conference held at Huntsville, Alabama, Sept. 22-24, 1993.

[9] R.S. Snyder (ed.), Second International Microgravity Laboratory (IML-2) Final Report, NASA TM-XXXXX, 1997, (in press). (Proceedings of the IML-2 Investigators Annual Meeting, ESRIN, Frascati, Italy, Nov., 7-8, 1995.)

[10] B.S. Singh, Third Microgravity Fluid Physics Conference, NASA Conference Publication 3338, Workshop Proceedings, Cleveland, Ohio, July 13–15, 1996.

[11] D. Langbein, Fluid statics and dynamics in microgravity, *J. Phys.: Condens. Matter*, **2**, SA491 (1990).

[12] P. Concus, Static menisci in a vertical right circular cylinder, *J. Fluid Mech.* **34**, 481 (1968).

[13] P. Concus, Capillary stability in an inverted rectangular tank, LMSC, *Advances in the Astronautical Sciences*, **14**, 21 (1963).

[14] J.G. Seebold, M.P. Hollister, H.M. Satterlee, Capillary hydrostatics in annular tanks, *J. Spacecraft*, **4**, No. 1, Jan. (1967).

[15] W.J. Masica, D.A. Petrash, Hydrostatic stability of the liquid-vapor interface in a gravitational field, NASA TN D-2267, (1965).

[16] W.J. Masica, J.D. Derdul, D.A. Petrash, Hydrostatic stability of the liquid-vapor interface in a low-acceleration field, NASA TN D-2444, (1964).

[17] D. Langbein, R. Großbach, W. Heide, Parabolic flight experiments on fluid surfaces and wetting, *Appl. Microgravity Tech.*, **II**, No. 4, 198 (1990).

[18] D.A. Petrash, R.C. Nussle, E.W. Otto, Effect of contact angle and tank geometry on the configuration of the liquid-vapor interface during weightlessness, NASA TN D-2075, October, (1963).

[19] B.N. Agrawal, Dynamic behavior of liquids on spacecraft attitude control, Proc. First INTELSAT/ESA Symposium, WA, D.C. April 25-26, 1984.

[20] B.A. Smith, Five iridium satellites placed in orbit, *Aviation Week & Space Technology*, May 12, 25 (1997).

[21] J.C. Slattery, *Interfacial Transport Phenomena*, [Springer-Verlag, New York, 1990]. For physical mechanisms see p. 107, for contact angle measurements see p. 179 and references cited.

[22] S.F. Kistler, Hydrodynamics of wetting, in *Wettability*, Surfactant Science Series, **49**, ed. J.C. Berg, [Marcel Dekker, Inc., New York, 1993], p. 311.

[23] E.B. Dussan V, On the spreading of liquids on solid surfaces: static and dynamic contact lines, *Ann. Rev. Fluid Mech.*, **11**, 371 (1979).

[24] J. Koplik, J.R. Banavar, Continuum deductions from molecular hydrodynamics, *Annu. Rev. Fluid Mech.*, **27**, 257 (1995).

[25] J. Israelachvili, *Intermolecular & Surfaces Forces*, [Academic Press Inc., San Diego, 1992], chpt. 15.

[26] Y.D. Shikhmurzaev, The moving contact line on a smooth solid surface, *Int. J. Multiphase Flow*, **19**, No. 4, 589 (1993).

[27] G.F. Teletzke, Thin liquid films: molecular theory and hydrodynamic implications, Ph.D. thesis, Univ. Minnisota, Minneapolis, 1983.

[28] G.W. Young, S.H. Davis, A plate oscillating across a liquid interface: effects of contact-angle hysteresis, *J. Fluid Mech.*, **174**, 327 (1987).

[29] L.M. Hocking, The damping of capillary-gravity waves at a rigid boundary, *J. Fluid Mech.*, **179**, 253 (1987).

[30] Y. Kamotani, L. Chao, S. Ostrach, H. Zhang, Effect of g jitter on free-surface motion in a cavity," *J. of Spacecraft and Rockets*, **32**, No. 1, 177 (1995).

[31] E.B. Dussan V, E. Rame, S. Garoff, On identifying the appropriate boundary conditions at a moving contact line: an experimental investigation, *J. Fluid Mech.*, **230**, 97 (1991).

[32] C.L. Ting, M. Perlin, Boundary conditions in the vicinity of the contact line at a vertically oscillating upright plate: an experimental investigation, *J. Fluid Mech.*, **2**, 263 (1995).

[33] P.H. Steen, Capillary and interfacial phenomena, wetting and spreading, in *Research Trends in Fluid Dynamics*, eds. J.L. Lumley, A. Acrivos, L.G. Leal, S. Leibovich, [AIP Press, Woodbury, New York, 1996], p. 286.

[34] J. Lekan, D. Gotti, A.J. Jenkins, J.C. Owens, M.R. Johnston, Users guide for the 2.2 second drop tower of the NASA Lewis Research Center, NASA TM 107090, April 1996.

[35] C.E. Siegert, D.A. Petrash, E.W. Otto, Time response of liquid-vapor interface after entering weightlessness, NASA TN D-2458, 1964.

[36] T. E. Bowman, Cryogenic liquid experiments in orbit, Vol. 1: liquid settling and interface dynamics, NASA CR-651, 1965.

[37] H.R. Ross, A.D. Pline, Equilibrium times for gas-liquid systems exposed to step changes in gravity, AICHE Ann. Mtg., WA DC, Dec. 1988.

[38] M.M. Weislogel, H.D. Ross, Surface reorientation and settling in cylinders upon step reduction in gravity, *Microgravity Sci. Technol.* **III**, No. 1, 24 (1990).

[39] G. Wölk, M. Dreyer, H.J. Rath, M.M. Weislogel, Damped oscillations of a liquid/gas surface upon step reduction in gravity, *J. of Spacecraft and Rockets*, **34**, No. 1, 110 (1997).

[40] P.J. Haley, M.J. Miksis, Dissipation and contact-line motion, *Phys. Fluids A*, **3**, No. 3, 487 (1991).

[41] J.A. Salzman, W.J. Masica, Lateral sloshing in cylinders under low gravity conditions, NASA TN D-5058, 1969.

[42] W.F. Kaukler, Fluid oscillation in the drop tower, *Metallurgical Transactions*, **19A**, 2625 (1988).

[43] M.P. Hollister, H.M. Satterlee, H. Cohan, Liquid propellant behavior during periods of varying accelerations, Rep. LMSC/A874728 (NASA-CR-92082), Lockheed Missiles and Space Co., 1967.

[44] M. Chaudhury, G.M. Whitesides, How to make water run uphill, *Science*, **256**, 1539 (1992).

[45] P. Concus, R. Finn, Capillary surfaces in microgravity, in *Low-Gravity Fluid Dynamics and Transport Phenomena*, **130**, Progress in Astronautics and Aeronautics, [AIAA Inc., Washington DC, 1990], p. 183.

[46] D. Langbein, Liquid surfaces in polyhedral containers, *Microgravity Sci. Technol.*, **VIII**, No. 3, 148 (1995).

[47] A.D. Myshkis, V.G. Babskii, N.D. Kopachevskii, L.A. Slobozhanin, A.D. Tyuptsov, *Low-Gravity Fluid Mechanics*, [Springer-Verlag, New York, 1987].

[48] M.M. Weislogel, Spontaneous steady capillary flow in partially coated tubes, *AIChE J.*, **43**, No. 3, 645 (1997).

[49] D. Langbein, M. Weislogel, Dynamics of liquids in edges and corners (DYLCO): an IML-2 experiment for the BDPU, Second International Microgravity Laboratory (IML-2) Final Report, ed. R.S. Snyder, NASA TM XXXXX, 1997. (in press)

[50] H. Wong, S. Morris, C.J. Radke, Three-dimensional menisci in polygonal capillaries, *J. Colloid and Int. Sci.*, **148**, No. 2, 317 (1992).

[51] P. Concus, R. Finn, On the behavior of a capillary free surface in a wedge, *Proc. Nat. Acad. Sci. U.S.A.*, **63**, 292 (1969).

[52] M.M. Weislogel, Capillary flow in an interior corner, Ph.D. Thesis, Northwestern Univ., June, 1996.

[53] A. de Lazzer, D. Langbein, M. Dreyer, H.J. Rath, Mean curvature of liquid surfaces in arbitrary shaped vessels, *Microgravity Sci. Technol.*, (1997). (to appear)

[54] F.J. Mayer, J.F. McGrath, J.W. Steele, A class of similarity solutions for the nonlinear thermal conduction problem, *J. Phys. A: Math. Gen.*, **16**, 3393 (1983).

[55] B. Legait, Laminar flow of two phases through a capillary tube with variable square cross-section, *J. Colloid and Int. Sci.*, **96**, No. 1, (1983).

[56] T.C. Ransohoff, P.A. Gauglitz, C.J. Radke, Snap-off of gas bubbles in smoothly constricted noncircular capillaries, *AIChE J.*, **33**, No. 5, 753 (1987).

[57] M.M. Weislogel, S. Lichter, A spreading drop in an interior corner: theory and experiment, *Microgravity Sci. Technol.*, (1997) (to appear)

[58] M. Dong, I. Chatzis, The imbibition and flow of a wetting liquid along the corners of a square capillary tube, *J. Colloid and Int. Sci.*, **172**, 278 (1995).

[59] M. Dreyer, A. Delgado, H.J. Rath, Capillary rise of a liquid between parallel plates under microgravity, *J. Colloid Int. Sci.*, **163**, No. 1, 158 (1994).

[60] P. Concus, R. Finn, M. Weislogel, Drop-tower experiments for capillary surfaces in an exotic container, *AIAA J.*, **3**, 134 (1992).

[61] C.A. Ward, D. Yee, M.R. Sasges, L. Pataki, D. Stanga, Configurational stability of fluid systems in near weightlessness, Winter Ann. Mtg. of ASME, AMD-Vol. 154, FED-Vol. 142, 111 (1992).

[62] P. Concus, R. Finn, M. Weislogel, Flight results of the interface configuration experiment USML-1/Mir, (in preparation) (compare with [60])

[63] P. Concus, R. Finn, M. Weislogel, Flight results of the interface configuration experiment USML-2; proboscis vessels, (in preparation)

[64] A. Chen, P. Concus, R. Finn, M. Weislogel, On cylindrical container sections for a capillary free-surface experiment, *Microgravity Sci. Technol.* (1997) (to appear)

Figure Captions

1. Equilibrium interface shapes in circular cylinder for $Bo \ll 1$ for a variety of contact angles θ. Enlarged region exemplifies complexities at contact line on a sub-microscale.

2. Sketch of equilibrium interface shapes in circular cylinder of radius R for normal-g, $Bo \gg 1$, and for low-g, $Bo \ll 1$, with a perfectly wetting liquid ($\theta = 0$). Enlarged region identifies capillary length L_c for gravity dominated interface only; for low-g interface $L_c = R$.

3. Results of drop tower tests showing meniscus centerline location Z vs. time t for silicone oil fluids in circular cylinders of radius $R = 9.52$ mm. (a) Effect of viscosity with $\theta = 0$. (b) Effect of contact angle at two different viscosities.

4. Dimensionless settling time $\mu t_s (1 + \Theta^2)/\rho R^2$ vs. correlation $10^B \zeta^A + 0.01\Theta^2$ for complete set of drop tower tests for property ranges $9.52 \leq R \leq 30($ mm$)$; $0.0005 \leq \mu \leq 0.5$ kg/m·s; $760 \leq \rho \leq 1238$ kg/m^3; $0.0159 \leq \sigma \leq 0.0695$ N/m; and $0° \leq \theta \leq 70°$. A=Acrylic and FC=flourochemically coated acrylic.

5. Effect of (discontinuous) variation in surface wettability in partially filled spherical tank: left side internal surface of tank is treated so that contact angle θ is large; for right side surface $\theta = 0$. (a) Normal-g surface. (b) Low-g surface.

6. Steady flow resulting from a pressure gradient in circular tube of constant radius R whose left side exhibits a less wetting condition than does the right side, where $Bo \ll 1$ and $\theta_1 < \theta_2$. (a) No flow. (b) Steady flow. (c) No flow.

7. Axial location of advancing meniscus centerline Z vs. time for a liquid slug in discontinuously wetted tube for a variety of liquid slug lengths l. Tube data: $R = 0.258$ mm, $L = 95$ mm. Silicone oil data: $\mu = 0.0008$ kg/m·s; $\rho = 816$ kg/m^3; $\sigma = 0.0174$ N/m; static value $\theta_1 = 0$; static value $\theta_2 \doteq 36°$. Time $t = 0$ here represents initiation of data collection, not beginning of flow.

8. $V/\Delta \cos\theta$ vs. $a\sigma/\mu$ for steady capillary flows caused by wetting discontinuity in tubes. Capillary tubes tested horizontally at normal-g with various surface preparations; U-tubes tested in low-g environment of a drop tower. Parametric ranges for tube dimensions: $0.258 \leq r \leq 4.94$ mm; $6 \leq l \leq 134$ mm; $95 \leq L \leq 481$ mm. Silicone oil fluids: $0.0005 \leq \mu \leq 0.1$ kg/m·s; $760 \leq \rho \leq 964$ kg/m^3; $0.016 \leq \sigma \leq 0.021$ N/m. Static value for θ_1 was 0 for all tests performed and the static value for θ_2 varied, $31° \leq \theta_2 \leq 60°$.

9. General equilibrium interface configurations in square cross-sectioned container (shown bisected along diagonal) for various contact angle ranges. (a) Normal-g, $Bo \gg 1$, for all θ. (b) Low-g, $0 \geq \theta \leq 45°$. (c) Low-g, $45° < \theta < 135°$. (d) Low-g, $135° \leq \theta \leq 180°$. Liquid phase is cross hatched along diagonal bisector.

10. (a) Surface profiles at select times showing capillary rise in a cylinder of equilateral triangular cross-section after a step reduction in gravity during a drop tower test: $t = 0, 0.2, 0.4$, and 1.0 s. Container data: $\alpha = 30°$; face width $D = 22.6$ mm. Silicone oil: $\mu = 0.002$ kg/m·s; $\rho = 872$ kg/m^3; $\sigma = 0.02$ N/m; $\theta = 0$. (b) Overlay of digitized surface traces shown in Figure 10(a). H is the approximate constant height location ($z \equiv 0$) given by Eq. (20).

11. Surface $S(y, z, t)$ computed by using Eq. (21) at times $t = 0, 0.2, 0.4$, and 1.0 s: $\mu = 0.002$ kg/m·s; $\sigma = 0.02$ N/m; $\theta = 0$; $\alpha = 30°$; and $D = 22.6$ mm yielding $H = 3.7$ mm by way of Eq. (20). Compare with drop tower experiment results of Figure 10.

12. Static, metastable interface shapes during a critical proboscis container test in the Space Shuttle [63]. (a) Initial static interface after fill, the surface shape of which is identical to a drop tower test result [64]. (b) Interface shape after nearly 15 minutes and spurious disturbances imparted to container by crew member. Fluid is red-dyed aqueous ethanol, 50% by volume, in an acrylic container; $\theta = 32° \pm 2°$.
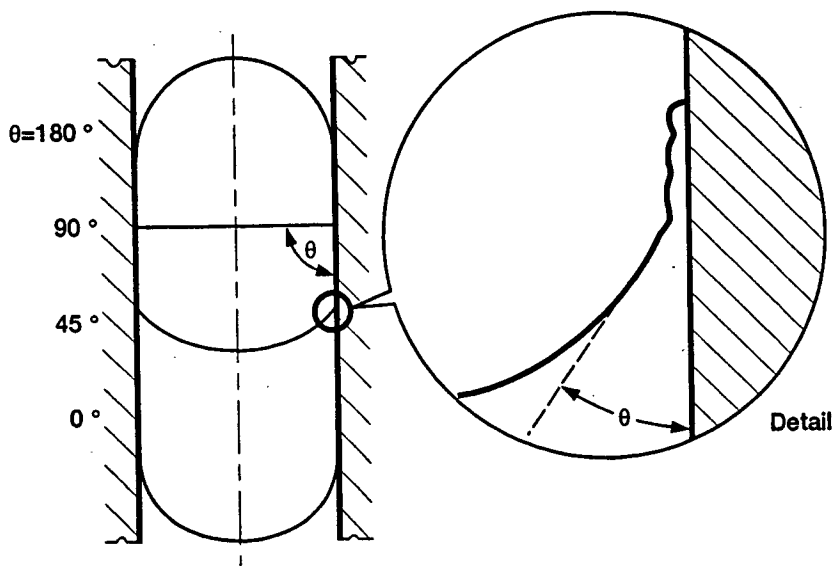
Figure 1
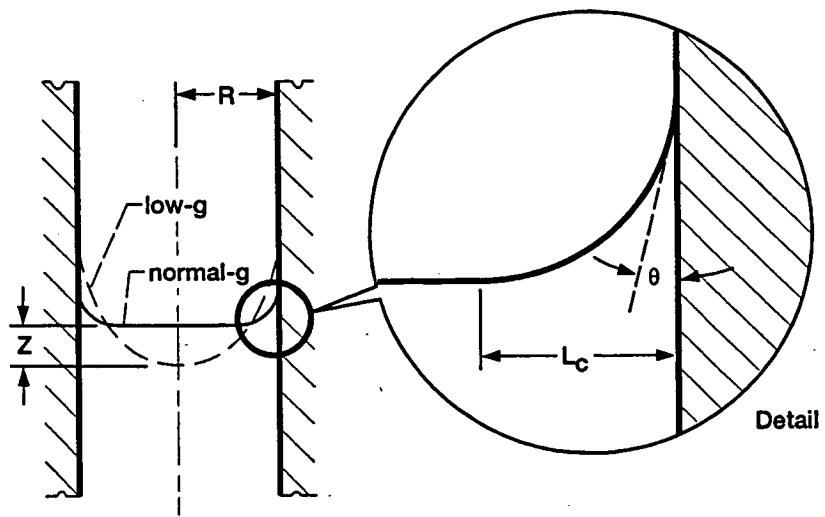
Figure 2
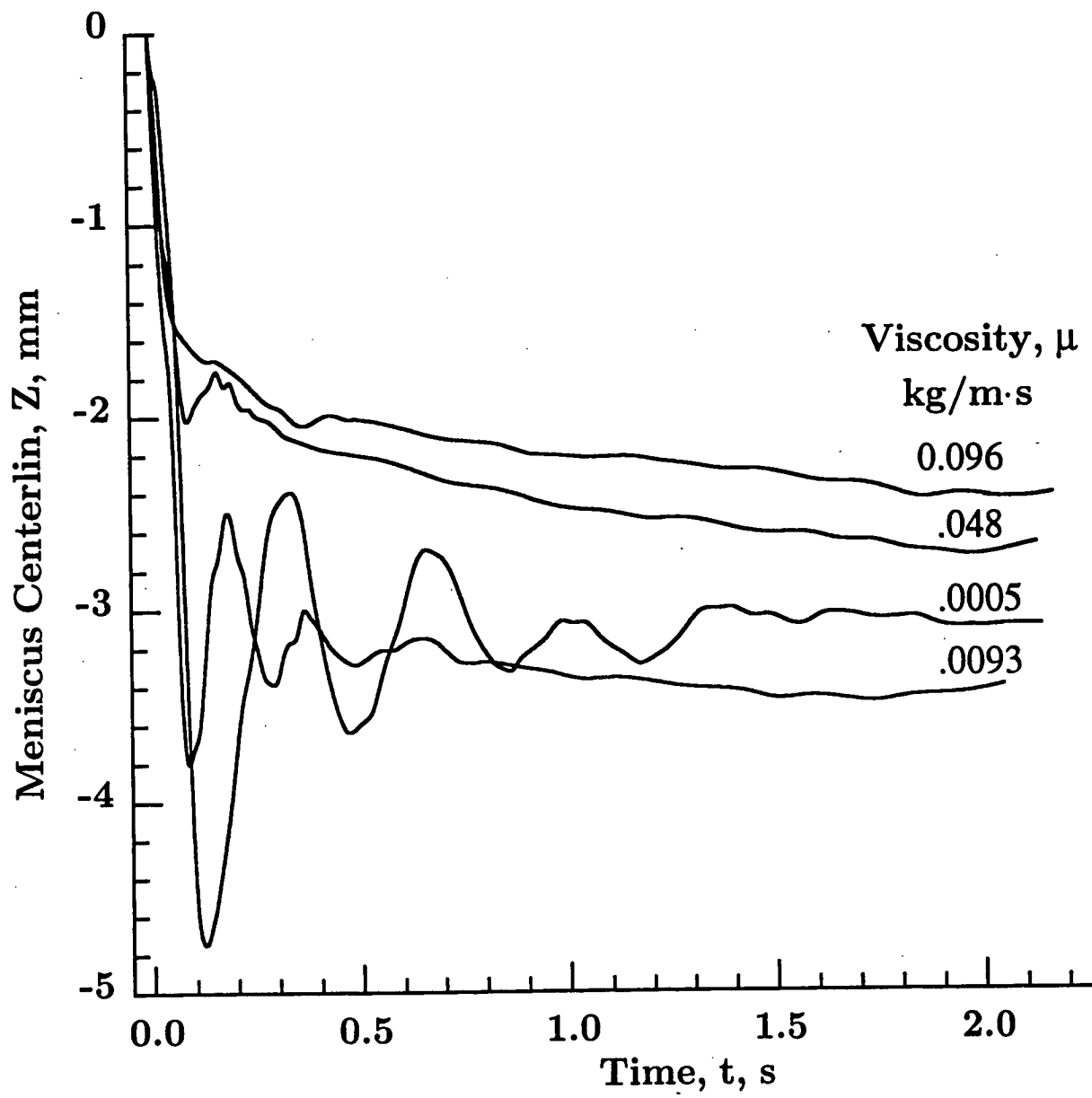
Fig. 3(a)
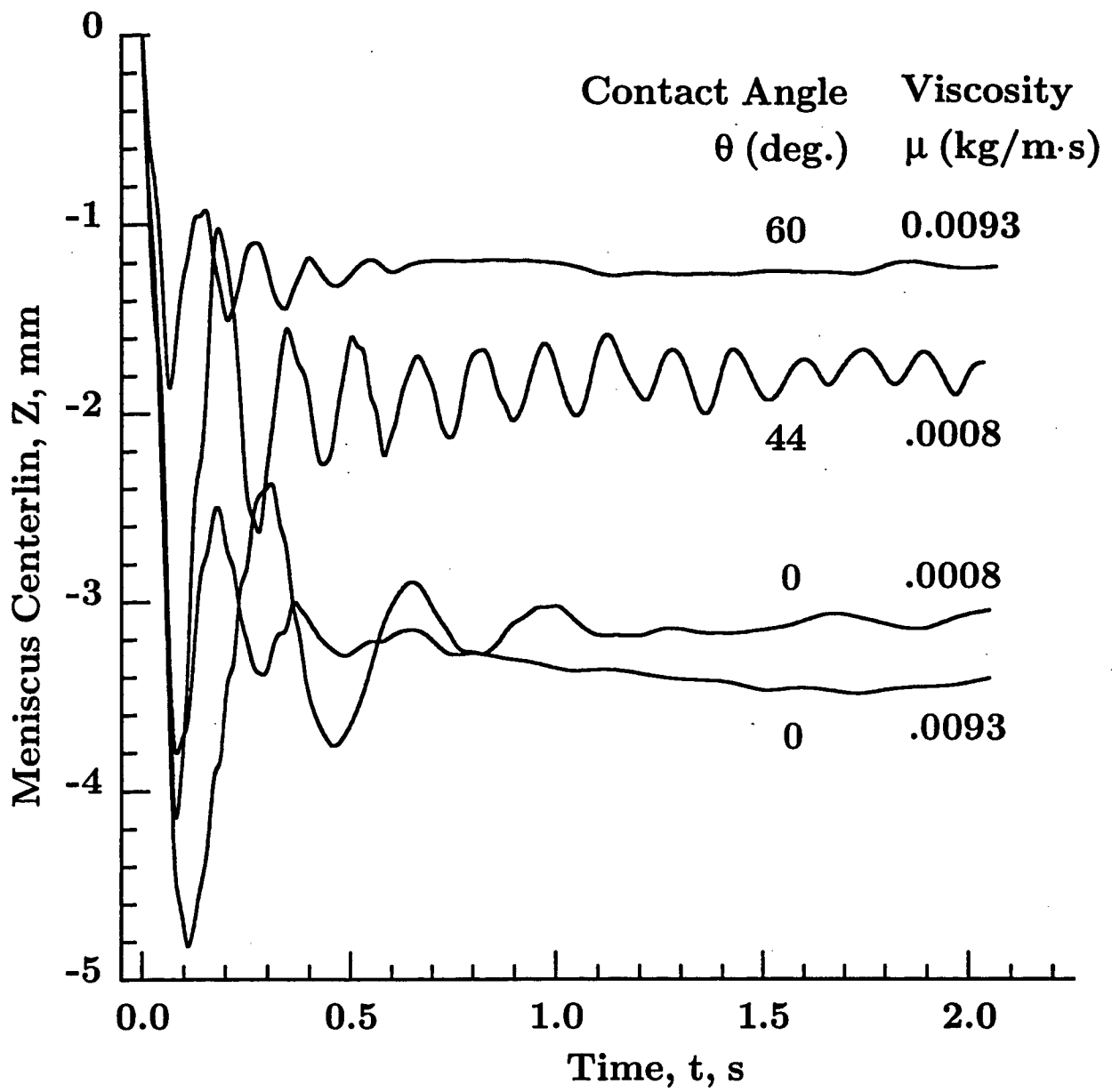
Fig. 3(b)
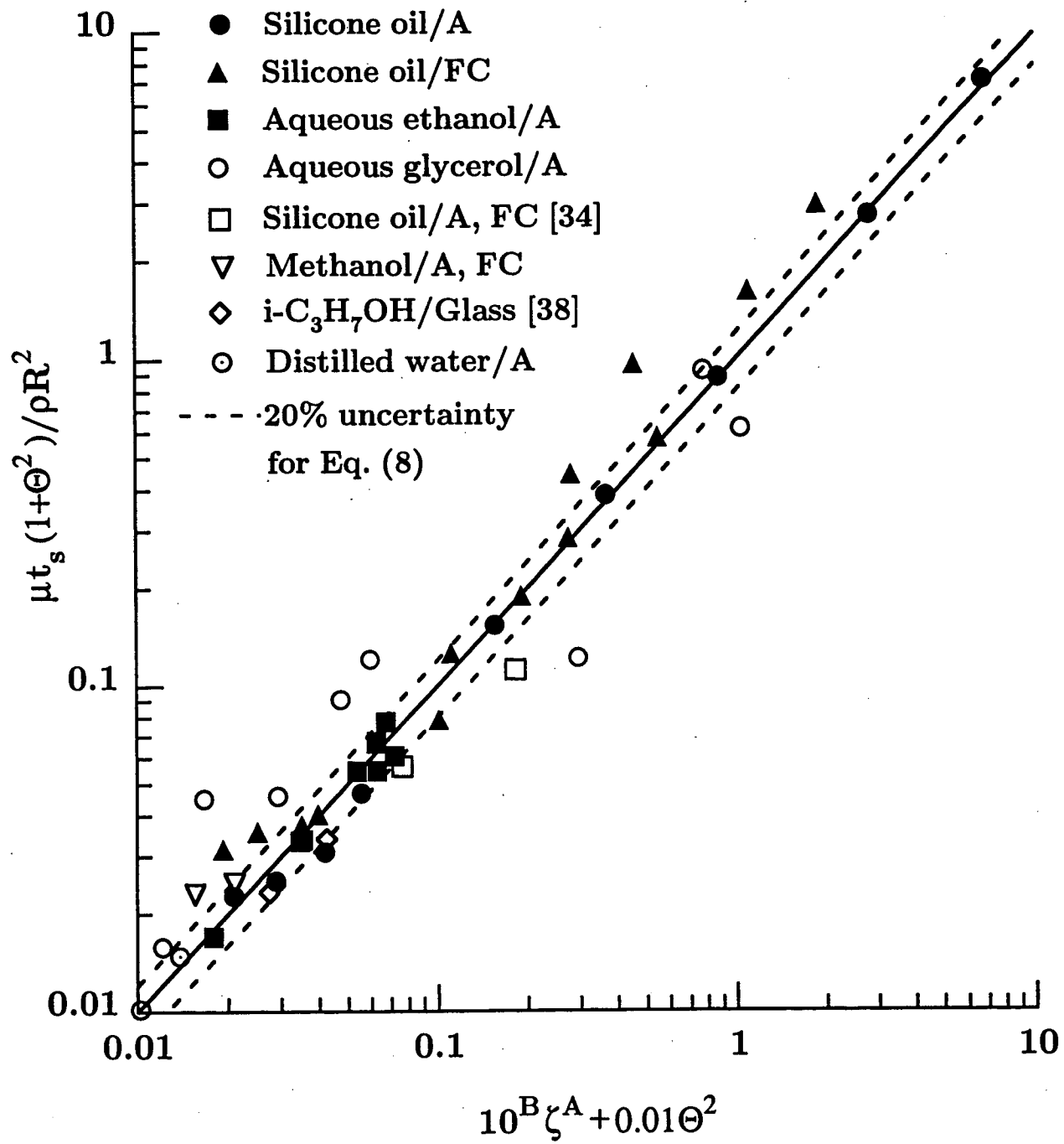
Fig 4
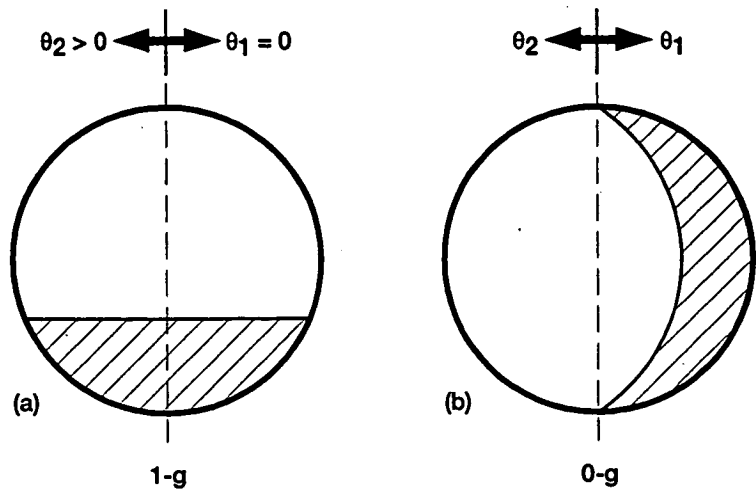
Figure 5

Figure 6

Fig. 7

Fig. 8

(a)   (b)   (c)   (d)

Figure 9

Fig. 10

(a)

(b)

Fig. 11

(a)   (b)

Fig. 12